LANGMUIR

pubs.acs.org/Langmuir Article

Structural Changes in Films of Pulmonary Surfactant Induced by Surfactant Vesicles

Konstantin Andreev, Michael W. Martynowycz, Ivan Kuzmenko, Wei Bu, Stephen B. Hall, and David Gidalevitz*

Cite This: *Langmuir* 2020, 36, 13439−13447 Read Online

ACCESS | Metrics & More | Article Recommendations | Supporting Information

ABSTRACT: When compressed by the shrinking alveolar surface area during exhalation, films of pulmonary surfactant *in situ* reduce surface tension to levels at which surfactant monolayers collapse from the surface *in vitro*. Vesicles of pulmonary surfactant added below these monolayers slow collapse. X-ray scattering here determined the structural changes induced by the added vesicles. Grazing incidence X-ray diffraction on monolayers of extracted calf surfactant detected an ordered phase. Mixtures of dipalmitoyl phosphatidylcholine and cholesterol, but not the phospholipid alone, mimic that structure. At concentrations that stabilize the monolayers, vesicles in the subphase had no effect on the unit cell, and X-ray reflection showed that the film remained monomolecular. The added vesicles, however, produced a concentration-dependent increase in the diffracted intensity. These results suggest that the enhanced resistance to collapse results from enlargement by the additional material of the ordered phase.

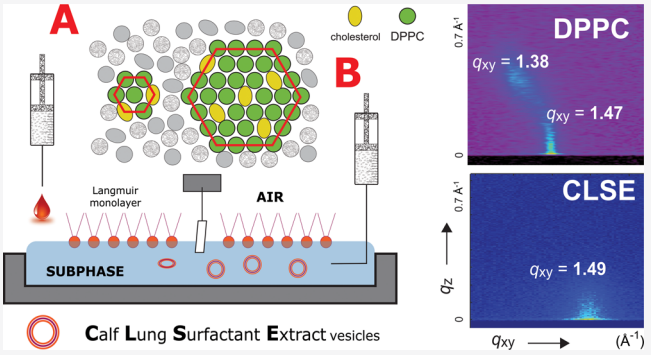

INTRODUCTION

Pulmonary surfactant is the combination of lipids and proteins that lowers surface tension (γ) in the lungs.[1] The material forms a thin film on the surface of the liquid that lines the alveolar air sacs.[2] When compressed by the decreasing interfacial area during exhalation, the films reduce γ to exceptionally low values, below 5 mN·m^{-1}.[3−8] This function of pulmonary surfactant is essential for normal breathing. Premature infants[9] and experimental animals[10] that lack adequate amounts of surfactant have lungs that are initially anatomically normal. The barrier that prevents flow of fluid from capillary blood to the alveolar air space is thin, consisting largely of four cellular membranes.[11] Breathing with elevated γ injures that barrier, increasing its permeability and resulting in pulmonary edema.

The low γ in the lungs indicates that the alveolar films avoid a phase transition. At the equilibrium spreading tension (γ_e) (~25 mN·m^{-1} for fluid-phase phospholipids),[12,13] the two-dimensional monolayer coexists with its three-dimensional bulk phase.[14] Attempts to increase the interfacial density further, either by adding constituents or by decreasing the area, produce at most a transient decrease in γ. Constituents flow from the interface to produce more of the smectic bulk phase and restore the γ_e.[15] Films that exist for prolonged periods at γ below γ_e are not at equilibrium. The γ's in the lungs, which are well below γ_e, indicate that the alveolar films are metastable. To sustain the low γ, the films must have the resistance to flow from the interface that defines a solid.[16,17]

The most fundamental question of how pulmonary surfactant achieves its remarkable function remains unanswered. The structure of the alveolar film that enables it to resist collapse remains unknown. The nature of the film during the initial stages of adsorption is clear. At $\gamma > \gamma_e$, vesicles of surfactant insert into the surface as collective packets,[18−20] delivering their complete set of constituents to form a monomolecular film. These initial monolayers are incapable of replicating the performance of the alveolar film. At physiologic temperatures, and during the quasi-static compressions that reduce alveolar γ to low levels,[21,22] monolayers with the full complement of surfactant constituents collapse at γ_e.[17] Some additional processes must convert the initial adsorbed monolayer to a film that resists collapse.

A series of models propose different mechanisms by which this conversion might occur and different resulting structures that could sustain low γ.[1,23−26] The studies here consider the changes induced by material in the subphase beyond the

Received: June 18, 2020
Revised: September 22, 2020
Published: October 20, 2020

https://dx.doi.org/10.1021/acs.langmuir.0c01813
Langmuir 2020, 36, 13439−13447

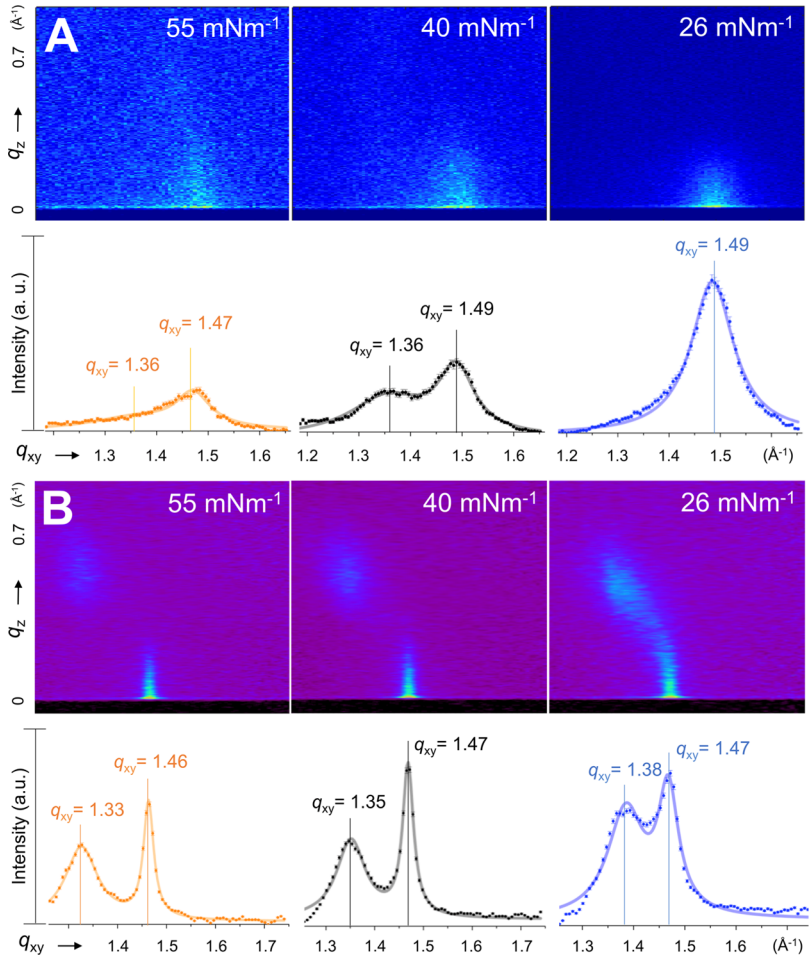

Figure 1. GIXD from monolayers of (A) CLSE and (B) DPPC spread from organic solvent and compressed to different γ. The upper row gives the imaged intensities. The lower row provides the variation of intensities integrated over q_z. Continuous curves represent the best fits to the data using Lorentz−Gauss crossed peaks. Symbols give mean ± SD, with errors assumed to be Poisson-distributed.

Table 1. Lateral Organization of Crystalline Regions (γ = 26−28 mN·m^{-1})[a]

	d-spacing (Å ± 0.01)	a, b (Å ± 0.1)[b]	A_{UC} (Å^2 ± 0.1)	τ (deg)
CLSE	4.22	4.87	20.6	0
DPPC	$d_{(1,1),(1,-1)}$ = 4.55	a = 5.37	44.2[c]	32
	$d_{(0,2)}$ = 4.27	b = 8.54		0
DPPC/Chol 3:1	4.27	4.93	21.1	0

[a]Constituents were spread from chloroform to high γ and compressed. A_{UC}—area per unit cell; Chol—cholesterol; τ—angle of molecular tilt from the surface normal. [b]For a centered rectangular unit cell, dimensions $a \neq b$. For a hexagonal unit cell, $a = b$. [c]A_{UC} for DPPC contains two alkyl chains.

content of a monolayer at γ_e. Several laboratories have shown that pulmonary surfactant in the subphase can stabilize the surfactant films.[27−30] The effects of surfactant vesicles provide a reasonable explanation for how the initial monolayer becomes functional. The studies here used grazing incidence X-ray diffraction (GIXD) and X-ray reflectivity (XRR) to establish the structural alterations responsible for the functional change.

RESULTS AND DISCUSSION

Initial Monolayers of Calf Lung Surfactant Extract. Prior studies have shown that vesicles in the subphase, below the interface, improve the ability of compressed surfactant films to reach and sustain γ below γ_e.[27−30] To establish the structural changes causing this stabilization, we first determined the structure of the initial monolayer. Vesicles of pulmonary surfactant adsorb as collective entities,[18−20] forming initial monomolecular films that contain all components of the adsorbing vesicles.[31] We first established the structure of compositionally well-defined monolayers of calf lung surfactant extract (CLSE). Solutions of CLSE in chloroform deposited at low interfacial densities formed monomolecular films. These Langmuir films have served as a model of the initial alveolar film since the earliest research on pulmonary surfactant.[32] Compression on a Langmuir trough varied the interfacial density and surface tension. GIXD provided structural information.

Diffraction first occurred at γ = 55 mN·m^{-1} (Figure 1A). The intensities were best fitted by two broad distributions centered at q_{xy} = 1.36 and 1.47 Å^{-1}. This pattern corresponded

https://dx.doi.org/10.1021/acs.langmuir.0c01813
Langmuir 2020, 36, 13439−13447

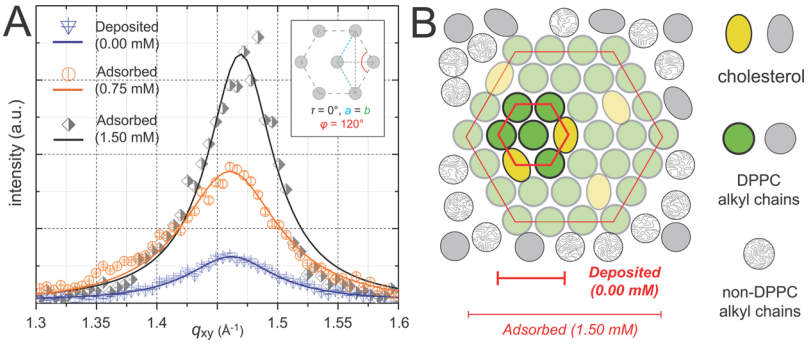

Figure 2. Effect of the subphase material on the diffracted intensity. (A) GIXD from CLSE films at γ = 26 mN·m^{-1}. Adsorbed films formed from dispersed vesicles injected below a clean interface to achieve the final concentrations indicated in brackets. Deposited films were formed by adding droplets of the dispersed material on the air/water interface. The dispersion had the same concentration and volume that was added to the subphase to reach the concentration there of 1.50 mM phospholipid. Symbols indicate experimental measurements with errors assumed to have Poisson distributions. Continuous curves give the best fit of Lorentz−Gauss peak functions to the data after subtraction of background. Fits were weighted by their statistical significance. The diagram in the insert represents the unit cell of the hexagonal lattice. a, b, and φ = parameters of the unit cell; τ = angle of molecular tilt from the surface normal. (B) Cartoon illustrating a possible arrangement of lipids within the crystalline domains (colored) and in the surrounding disordered phase (gray).

Table 2. Effect of Subphase Material on Adsorbed CLSE Films (γ = 26 mN·m^{-1})

CLSE subphase concentration (mM)[b]	d-spacing (Å ± 0.01)	a, b (Å ± 0.1)	A_{UC} (Å^2 ± 0.1)	L_{xy}[a] (Å ± 2)	total intensity (a.u.)
0.00	4.30	4.97	21.4	65	207 ± 14
0.75	4.30	4.97	21.4	58	693 ± 26
1.50	4.27	4.93	21.1	87	868 ± 29

[a]L_{xy}—in-plane coherence length. [b]Phospholipid concentration.

to a centered rectangular unit cell containing two acyl chains,[33] with dimensions of a = 8.54 Å and b = 5.45 Å and an area per alkyl chain of 23.3 Å^2. Diffraction was centered at q_z = 0 Å^{-1}, both here and at other γ, indicating the absence of molecular tilt between the nearest neighbor alkyl chains. Further compression to γ = 40−45 mN·m^{-1} increased the intensities and slightly reduced the size of the unit cell, but preserved the space group. At γ = 26 mN·m^{-1}, the pattern had changed (Figure 1A). A single peak at q_{xy} = 1.49 Å^{-1} indicated conversion to a hexagonal unit cell,[33] where a = b = 4.87 Å with an area per unit cell of 20.6 Å^2 (Table 1). This distinct structural shift has gone undetected in the numerous compression isotherms published previously for this multicomponent mixture.[34,35]

The classical model of pulmonary surfactant has long contended that the functional component of the alveolar film is a tilted-condensed (TC) monolayer.[36−38] The alkyl chains in that structure form a two-dimensional crystalline lattice.[39] The films readily sustain γ well below γ_e. At 37 °C, dipalmitoyl phosphatidylcholine (DPPC), which is the most prevalent constituent of pulmonary surfactant from most animals,[40] is the only component that forms the TC phase above γ_e. The model predicts that ordered regions in films of pulmonary surfactant resist collapse and consist of TC DPPC. We therefore compared our results from CLSE with GIXD from spread monolayers of DPPC.

At 55 mN·m^{-1}, GIXD from DPPC produced the expected two pronounced peaks at q_{xy} ≈ 1.33 and 1.46 Å^{-1} (Figure 1B), in agreement with previously published results.[41] This pattern corresponded to a centered rectangular unit cell with dimensions of a = 5.2 Å and b = 8.5 Å, and an area of 44.2 Å^2, or 22.1 Å^2 per alkyl chain. In contrast to the pattern for CLSE, the shift of the second peak off the plane (q_z ≈ 0.7 Å^{-1}) indicated tilt of acyl chains toward nearest neighbors.[33]

Compression to γ = 26 mN·m^{-1} produced a partial merger of the two peaks, suggesting a decrease in the d-spacing of the (1,1) and (1,−1) planes from 4.72 to 4.55 Å (Table 1). The angle of molecular tilt also decreased. A transition to a hexagonal unit cell did not occur. At the γ just above γ_e, at which fluid films collapse, the diffraction patterns for ordered regions of CLSE and TC DPPC indicated different structures and suggested distinct compositions.

Prior studies have suggested that ordered domains in monolayers of CLSE contain cholesterol as well as DPPC.[42,43] Measurements of GIXD determined if cholesterol/DPPC mixtures could mimic the structure of ordered regions in CLSE.[41] At $\gamma \approx \gamma_e$, GIXD from DPPC with 25 mol % cholesterol closely approximated the signal from CLSE (Figure S1). A single diffraction peak at q_{xy} = 1.47 Å^{-1} and q_z ≈ 0 Å^{-1} indicated alkyl chains hexagonally packed with a unit cell of a = b = 4.93 Å and an area per unit cell (A_{UC}) of 21.1 Å^2, without detectable molecular tilt (Table 1). Reducing the cholesterol ratio to 20% shifted the diffraction peak toward higher q_{xy} (Figure S1). The out-of-plane diffraction revealed the coherence length L_z of ∼13 Å, corresponding to the ordered portion of alkyl chains aligned with the cholesterol carbon rings. We made no attempt to define the range of cholesterol contents that would replicate the signal from CLSE. The results, however, supported the prior finding[42] that in addition to DPPC, the ordered regions of CLSE contained significant cholesterol.

Effect of Subphase CLSE. To determine how vesicles in the subphase affected the structure of the interfacial film, we first tested whether monolayers formed by depositing aqueous dispersions or solutions in chloroform at the surface had the same structure. Dispersed CLSE produced the same GIXD as the Langmuir films at the same γ. Diffraction again showed the single peak (Figure 2A) centered at q_z = 0, indicating a

https://dx.doi.org/10.1021/acs.langmuir.0c01813
Langmuir 2020, 36, 13439−13447

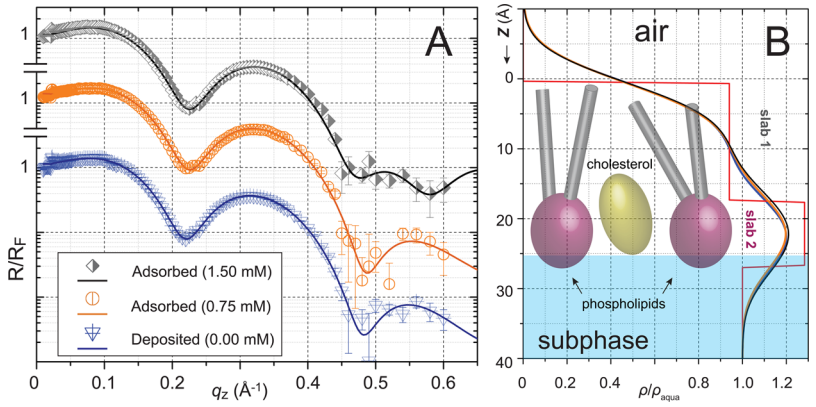

Figure 3. Effect of the subphase material on the transverse structure for films of CLSE. (A) XRR. Experiments measured the reflectivity from the same films used to obtain GIXD (Figure 2). The reflected intensity, R, is normalized relative to the Fresnel reflectivity, R_F, for an ideally flat air–water interface. Symbols give measured values, where vertical bars indicate the error assuming Poisson distributions about the counted intensity. The continuous curves give the best fit to the data by the Fourier transform of the two-slab model of electron density. (B) Electron density profiles, normalized relative to the electron density of the aqueous buffer ($\rho_{aqua} \sim 0.334$ e$^-$·Å^{-3}), derived from the data in (A). Z denotes the distance from the top of the upper slab (slab 1). The superimposed molecular cartoon suggests the general orientation of lipids in the monolayer.

Table 3. Two-Slab Model of CLSE Films Perpendicular to the Interface[a]

	slab 1 (non-polar)		slab 2 (polar)		
CLSE subphase concentration (mM)	l_n (Å)	ρ_n/ρ_{aqua}	l_p (Å)	ρ_p/ρ_{aqua}	interfacial roughness[b] σ (Å)
0.00	17.0 ± 0.07	0.94 ± 0.01	9.40 ± 0.15	1.28 ± 0.01	4.2 ± 0.1
0.75	16.7 ± 0.09	0.95 ± 0.01	9.14 ± 0.17	1.29 ± 0.01	4.3 ± 0.1
1.50	15.8 ± 0.09	0.94 ± 0.02	11.15 ± 0.17	1.26 ± 0.01	4.1 ± 0.1

[a] l and ρ are the thickness and electron density, respectively, of the nonpolar (subscript n) and polar (subscript p) homogeneous slabs. The values of ρ are normalized relative to that of the aqueous buffer ($\rho_{aqua} \sim 0.334$ e$^-$·Å^{-3}). Errors correspond to model uncertainty. [b] Roughness at all interfaces is set to be equal.

hexagonal lattice without molecular tilt. The dimensions (a = 4.97 Å) and d-spacing (4.30 Å) were slightly larger than the values for CLSE spread from organic solvent (Table 2), but the structures were basically comparable.

Films formed by adsorption of vesicles added below a clean interface had essentially the same local structure. GIXD again produced a single peak with minimal change in q_{xy} (Figure 2A) and no effect on q_z. The ordered regions retained a hexagonal unit cell with similar dimensions and untilted chains (Table 2). The total diffracted intensity, however, increased (Figure 2). With a concentration of 0.75 mM, the integrated intensity was more than threefold higher than the signal for the monolayer above an empty subphase (Table 2). The effect was concentration-dependent (Figure 2A). Doubling the subphase concentration to 1.50 mM increased the intensity further by 25% (Table 2). During exposure to an incident beam of equal intensity for equivalent durations, the area of an ordered structure should determine the diffracted intensity. Although material in the subphase had no effect on the molecular arrangement within ordered regions, the vesicles significantly increased their total area.

The presence of 1.50 mM CLSE in the subphase also decreased the width of the diffracted peak. The coherence length, L_{xy}, which indicates the average size of individual ordered domains, is inversely related to the width (see Experimental Section). The additional material increased L_{xy} by 50% (Figure 2B and Table 2). Our studies provided no information concerning the number of ordered regions. They offered no insight into whether subphase vesicles caused nucleation of new ordered domains. Our results did show that the increased ordered area occurred at least in part by growth of the existing domains.

Transverse Structure of Adsorbed CLSE. Microscopic studies showed decades ago that at least portions of the alveolar film have a multilamellar thickness.[18,44,45] If a greater thickness impedes collapse, then the formation of additional layers might produce a film more capable of sustaining low γ. Vesicles in the subphase might stabilize the initial monolayer by contributing additional layers. We used XRR to determine the thickness of the film and to test for the presence of an interfacial multilayer.

XRR provided the electron density along the normal to the interface (Figure 3). A simplified model of CLSE films as a stack of two horizontal, homogeneous slabs successfully fits all measured intensities (Figure 3A). The upper slab 1, which is closer to air, should contain the hydrophobic groups, such as the aliphatic chains of the phospholipids, cholesterol, and the palmitoylated N-terminus of SP-C, one of the hydrophobic surfactant proteins. Slab 2, adjacent to the aqueous subphase, should instead contain the hydrated phospholipid headgroups along with the polar moieties of the proteins. The electron densities for slab 1 varied from 0.314 to 0.317 e$^-$·Å^{-3} (0.94–0.95 relative to that of water, ρ_{aqua}) (Figure 3B). These values slightly exceeded the densities of 0.304 and 0.307–0.311 e$^-$·Å^{-3} for pure DPPC[46] and dipalmitoyl phosphatidylglycerol,[46,47] respectively. In turn, the densities of the polar slab 2, ranging within 0.428–0.431 e$^-$·Å^{-3} (1.26–1.29·ρ_{aqua}), were lower than the values for phospholipids (Table 3).[46−49] These differences seemed most likely to reflect the presence of cholesterol and the hydrophobic surfactant proteins in CLSE. The material added to the subphase had little or no effect on

https://dx.doi.org/10.1021/acs.langmuir.0c01813
Langmuir 2020, 36, 13439−13447

the density or thickness for either slab. The subphase vesicles therefore produced essentially no change in the total thickness of the films. For all measurements, the thickness of 26−27 Å (Table 3) indicated the presence of a monolayer. Similar to the lateral structure detected by GIXD, the material in the subphase had no detectable effect on the transverse structure.

Our studies have direct implications for the process by which vesicles of pulmonary surfactant in the subphase produce a concentration-dependent stabilization of surfactant films.[27−30] Our results show no change in the local structure. An ordered phase retains the same unit cell and dimensions and the same monomolecular thickness. Our results show instead that the conditions, which significantly stabilize surfactant films against collapse,[30] induce a major enlargement of the ordered phase.

The relationship of our findings to the alveolar film is indirect. By experimental necessity, we conducted our experiments at 23 °C. The functional studies demonstrating the stabilizing effects of the subphase material included measurements at the same temperature. The similar conditions allowed the correlation between the functional and structural changes. The subphase vesicles also stabilized films at 37 °C. We assume that the correlation between the structure and function at 23 °C extends to physiological temperatures.

Our results relate directly to two existing models of the functional alveolar film. Each predicts a functional structure that differs from the initial adsorbed monolayer. Each model predicts how vesicles in the subphase could promote conversion of the initial film to more stable structures. Each provides hypotheses that our methods test directly.

Our most definitive evidence concerns the multilamellar model. Our results contradict the prediction that vesicles in the subphase stabilize the film by forming a multilayer. Over the range of concentrations that slow collapse by 2 orders of magnitude,[30] the film remains monomolecular. The multilamellar films observed *in situ* seem more likely to result from collapse. When sufficiently compressed, phospholipid films collapse to form a stack of bilayers adjacent to the interface.[50,51] These multilayered structures, rather than deterring further collapse, provide the nidus at which additional compression forms towers of stacked bilayers above the surrounding monolayer.[50] The previously observed stabilizing effect of the subphase vesicles is evident at the outset of compression before significant collapse occurs.[27,30] These observations indicate that collapsed multilayers are unlikely to stabilize monolayers and that adsorbed multilayers are absent when stabilization occurs. Speculation that subphase vesicles achieve their stabilizing effect on monomolecular films by contributing additional layers appears unfounded.

Our results also address an aspect of the classical model, that the functional component of the alveolar film is a TC monolayer. The vesicles in the subphase that slow collapse might shift the film from some other initial, functionally incompetent structure to the TC phase. Our results show that the initial film at γ just above γ_e is not TC. Rather than the dual peaks of diffracted intensity from the centered rectangular lattice of the TC phase, monolayers of CLSE produce the single peak of a hexagonal lattice. The off-axis signal that indicates tilting of the acyl chains in TC films is absent with the initial films of CLSE. Without vesicles in the subphase, TC structures are undetectable in CLSE monolayers.

The material in the subphase that stabilizes the films produces no change in its local structure. The hexagonal lattice with untilted chains persists. The added material enlarges the ordered structure considerably, but that structure differs from the TC phase. Strictly speaking, the cardinal feature of the classical model is absent.

Our results agree with prior microscopic evidence that the ordered regions in CLSE differ from TC DPPC. Sufficient cholesterol converts the structure of DPPC monolayers.[41,52] The phospholipid accommodates the cholesterol in an ordered structure that diffracts, but the space group shifts, and the acyl chains lose their tilt.[41] The ordered regions in CLSE have these characteristics and closely resemble the structure of DPPC with 25% cholesterol. The prior microscopic studies yielded parallel results. Monolayers of the phospholipids in CLSE, without cholesterol or proteins, form coexisting phases.[53] The ordered domains contain only DPPC[53] and have the characteristics of the TC phase. Physiological levels of cholesterol convert the fixed domains with irregular borders to circular shapes that can reconfigure rapidly.[42] The solid, TC domains for the phospholipids alone change with the added cholesterol to a fluid structure.[42,54] Both the prior and current studies, using different experimental approaches,[42,55] conclude that the cholesterol in CLSE converts TC domains to a different structure.[56]

The ordered structure in CLSE that differs from a TC phase poses an important functional question. Growth of the ordered phase would stabilize the compressed film only if the ordered regions resist collapse. The characteristics of the ordered phase suggest that it may lack that feature. Collapse of a two-dimensional film into the third dimension indicates the ability to flow that defines a fluid.[16] In sufficient amounts, cholesterol induces films of DPPC to collapse.[57−59]

The destabilization of the compressed films has provoked the removal of cholesterol from most, but not all, therapeutic surfactants obtained from animal sources. The effect of cholesterol, however, is dose-dependent. Collapse becomes appreciable only above a threshold level.[60] We speculate that the level of cholesterol in the ordered phase of CLSE, which we consider incompletely defined by our studies, is below that threshold. The level may be sufficient to induce the previously observed two-dimensional fluidity without allowing collapse into the third dimension.

Growth of the ordered phase induced by surfactant vesicles solves a major problem with the classical model. DPPC dominates the content of the ordered regions that resist collapse, whether in the TC phase proposed by the original model or the ordered structure detected here. That compound commonly represents at most 35−40% of the surfactant phospholipids[61] and significantly less in some animals.[62] Formation of a TC film would require a major compositional change of the initial monolayer and enrichment of DPPC.

Earlier versions of the model invoked enrichment by selective exclusion. Compression below γ_e of coexisting solid and fluid phases causes collapse of the fluid regions. If compressed far enough, the result is a solid film.[36−38] At physiological temperatures, however, and γ just above γ_e, ordered domains in films of CLSE occupy ∼5% of the interface.[34] During a physiological compression, exclusion of fluid regions sufficient to produce a solid film seems unlikely. Physiological measurements of pulmonary mechanics also suggest that the newly formed alveolar film is competent to resist collapse before compression begins. Significant deflation of the lungs is apparently unnecessary to reach $\gamma < \gamma_e$, for example, refs.[4,5,8,21,63,64] Both observations argue against

https://dx.doi.org/10.1021/acs.langmuir.0c01813
Langmuir 2020, 36, 13439−13447

selective exclusion as the basis for forming an ordered alveolar film.

Our results suggest instead a compositional change by selective insertion. Material added to the subphase would provide a source of the components in the ordered phase, specifically including additional DPPC. Preferential partitioning of DPPC into the interfacial monolayer would enrich the film in that compound. Because the surfactant lipids fail to enter the interface close to γ_e in the absence of the hydrophobic surfactant proteins,[65,66] those constituents would presumably facilitate the partitioning. An ordered phase composed of DPPC with cholesterol could then grow. The stabilization of the interfacial film by material in the subphase is dose-dependent.[27,30] The concentration of the alveolar liquid is unknown but likely to be above 100 mM phospholipid,[27] which is 2 orders of magnitude more than the values used here. The extent of ordered regions in the alveolar film should be correspondingly greater.

The basis of partitioning would be thermodynamic rather than kinetic, but not from a difference in γ_e. Phospholipids above their main melting transition share a common γ_e of ∼24 mN·m^{-1}.[13,67] Phospholipids in solid structures adsorb poorly, suggesting that their γ_e may instead be just below the γ for a clean interface.[12,13] Insertion of compounds according to these γ_e would enrich the film in compounds that form fluid structures rather than DPPC. We speculate without evidence that constituents instead partition based on spontaneous curvature. DPPC, with its cylindrical shape, might prefer the relatively flat air−water interface over the curvature of undulating structures.

CONCLUSIONS

X-ray scattering from monolayers of pulmonary surfactant detects an ordered phase. DPPC with cholesterol in a molar ratio of ∼3:1, but not DPPC alone, mimics these ordered regions. Surfactant vesicles added below the surfactant film have no effect on the local structure, including its thickness and the unit cell of the ordered regions. The vesicles in the subphase, however, induce a substantial enlargement of the ordered phase in a concentration-dependent manner. The results argue that the previously observed stabilization of surfactant monolayers by surfactant vesicles in the subphase occurs not by the formation of multilayered structures but by growth of an ordered phase. That structure is distinct from TC DPPC, presumably because it contains significant amounts of cholesterol.

EXPERIMENTAL SECTION

Materials. DPPC and cholesterol were purchased from Avanti Polar Lipids (Alabaster, AL) and used without further purification or characterization. CLSE was obtained from ONY, Inc. (Amherst, NY). CLSE is prepared by centrifugal pelleting of large lipoprotein aggregates lavaged from freshly excised calf lungs,[68] followed by extraction of the particles with a nonpolar solvent.[69] Prior reports have published the detailed composition of CLSE.[65,70−73] For preparation of surfactant vesicles, evaporation of the solvent under a stream of nitrogen, followed by an overnight incubation in vacuum, yielded the dried lipid−protein mixtures. CLSE preparations were then resuspended in 4-(2-hydroxyethyl)-1-piperazineethanesulfonic acid (HEPES)-buffered saline (HS: 10 mM HEPES, pH 7.0, 150 mM NaCl) at a final phospholipid concentration of 32 mM (∼100 mg·mL^{-1}), followed by three cycles of sequential freezing and thawing (−80/23 °C), with vigorous vortexing before each freezing. Further sonication for 30 min in a water bath with ice yielded the final dispersion. Dynamic light scattering (ZetaPALS, Brookhaven Instruments Corporation, Nova Instruments LLC, Holtsville, NY) determined the size and polydispersity of freshly prepared liposomes to characterize the dispersions.

Formation of Interfacial Films. Our experiments used the air−water interface in a custom-built polytetrafluoroethylene (PTFE) Langmuir trough filled with HS containing calcium (HSC: 10 mM HEPES, pH 7.0, 150 mM NaCl, 1.5 mM $CaCl_2$) to mimic the surface of the liquid layer in an alveolus. The dimensions (76 × 76 × 3 mm) allowed the footprint of the beam incident at a grazing angle to avoid the edge of the trough. The volume of the buffer (25 mL) achieved a proud meniscus.

For well-defined monolayers, aliquots of chloroform solutions containing CLSE or specific lipids were spread onto the aqueous surface until γ fell slightly below 72 mN·m^{-1}. The films were then compressed using a PTFE barrier while monitoring γ with a Wilhelmy plate. GIXD was measured at regular intervals. Vesicles of CLSE, dispersed in HS, were either deposited as small droplets at the interface or injected into the subphase *via* an L-shaped needle below a clean interface. The CLSE added to the subphase, which formed films by adsorption, achieved final concentrations of 0.75 or 1.50 mM phospholipid. The dispersions deposited directly on the surface had the same concentration and volume used to produce the subphase concentration of 1.50 mM phospholipid.

Surface X-ray Scattering. X-ray measurements were conducted at either beamline 9-ID-C or 15-ID-C of the Advanced Photon Source at Argonne National Laboratory (Argonne, IL). A Langmuir trough was mounted in a hermetically sealed, helium-filled canister. The oxygen level, monitored continuously, was <1% to minimize background scattering. The temperature was at the ambient level of 23 °C for all experiments. The subphase was unstirred to minimize perturbation of the interface. Measurements collected data after the system achieved steady state. The exposures to the beam were 15−20 min for GIXD and 1.5 h for XRR.

Grazing Incidence X-ray Diffraction. GIXD provides information about the in-plane, lateral order of films. X-rays incident at a grazing angle penetrate only ∼100 Å below the surface[33] and are therefore sensitive to the monomolecular film rather than the bulk subphase. Measurements of GIXD used an X-ray beam with a wavelength (λ) of 0.92 Å (9-ID-C) or 1.24 Å (15-ID-B), striking the surface at an incident angle corresponding to 0.85% of the critical value (q_c = 0.0217 Å^{-1}). For an X-ray beam below the critical angle, intensity is a function of the momentum transfer parallel to the interface, q_{xy}. At an angle of 2θ between the incident and diffracted beams, q_{xy} is given by

$$q_{xy} = \frac{2\pi}{\lambda}\sin\left(\frac{2\theta}{2}\right)$$

The scattered intensity can be described in terms of diffraction from a large number of randomly oriented, two-dimensional crystalline domains. After subtracting linear background, the intensities were analyzed using OriginPro software (version 8.0, Northampton, MA) by fitting the data to a single Lorentz−Gauss (1:1) crossed peak. The q_{xy} of the peak yielded the repeat distances between the diffracting hydrocarbon chains

$$d_{h,k} = \frac{2\pi}{q_{xy}}$$

The breadth of the peak provided the coherence length, L_{xy}, of the diffracting region according to the Sherrer formula[74]

$$L_{xy} = 0.9\frac{2\pi}{\xi_{h,k}}$$

where $\xi = (\text{fwhm}^2 - \Delta^2)^{1/2}$ for the full width of the peak at the half-maximum (fwhm) and Δ is the resolution of the Soller slits. The acceptance of the Soller slits, fixed at 1.4 mrad, determined errors in q_{xy} (9.56 × 10^{-3} Å^{-1}).

The nearest neighbor tilt in our films follows the equation[75]

https://dx.doi.org/10.1021/acs.langmuir.0c01813
Langmuir 2020, 36, 13439−13447

$$q_z = qhk\hat{e}\tan(\tau)$$

where τ is the angle of molecular tilt along the **a** dimension of the unit cell,[33,76] indicated by $\hat{e}$.[77] The distribution of the diffracted intensities along q_z was analyzed using Python software by ChemMatCARS (the University of Chicago). The out-of-plane coherence length (L_z) has been calculated from the Bragg rod profile.[74]

Specular XRR. XRR determines the electron density profile across the interface. Measurements record the reflected intensities, expressed as a function of the wave vector perpendicular to the interface, q_z. For a beam incident on the surface at an angle α, q_z is given by

$$q_z = \frac{4\pi}{\lambda}\sin\alpha$$

The measured intensity of the reflected beam, corrected for the off-specular background, is normalized relative to the incident intensity. The beam's footprint limited the measurements of XRR to the range of q_z from 0.01 to 0.60 Å^{-1}. For determinations of the electron density profile, solutions to the phase problem used a model-independent approach. The interface was modeled as ∼50 discrete slabs, each with homogeneous electron density and a thickness of 1 Å. The program StochFit varied these slabs in order to match the measured reflectivity and maintain a smooth curve.[78] This continuous electron density was then fitted to a simplified model. Two slabs had discrete thicknesses (l), interfacial roughnesses (σ), and uniform densities (ρ), bounded by the known densities of the subphase (water) and superphase (air). Because of CLSE's compositional complexity, predicting the values of σ from prior studies on simple systems was impractical.[79] We therefore set σ to be identical at all interfaces, including between the two slabs and between the slabs and the adjacent phases. We then fit σ freely without constraint. This approach has been used successfully to study mimics of antimicrobial peptides,[47,80−82] the permeability of lipopolysaccharides in *Salmonella* spp.,[83,84] and surface catalysis.[85]

■ ASSOCIATED CONTENT

Supporting Information

The Supporting Information is available free of charge at https://pubs.acs.org/doi/10.1021/acs.langmuir.0c01813.

Lateral organization of crystalline regions (γ = 26−28 mN·m^{-1}) (PDF)

Effect of the subphase material on adsorbed CLSE films (γ = 26 mN·m^{-1}) (PDF)

Two-slab model of CLSE films perpendicular to the interface (PDF)

In-plane and out-of-plane diffraction on monolayers of CLSE and DPPC/cholesterol mixtures at the designated ratios (mol %) (PDF)

■ AUTHOR INFORMATION

Corresponding Author

David Gidalevitz − *Department of Physics, Center for Molecular Study of Condensed Soft Matter (μCoSM), Pritzker Institute of Biomedical Science and Engineering, Illinois Institute of Technology, Chicago, Illinois 60616, United States;* orcid.org/0000-0002-3620-780X; Email: gidalevitz@iit.edu

Authors

Konstantin Andreev − *Department of Physics, Center for Molecular Study of Condensed Soft Matter (μCoSM), Pritzker Institute of Biomedical Science and Engineering, Illinois Institute of Technology, Chicago, Illinois 60616, United States;* orcid.org/0000-0002-1757-4532

Michael W. Martynowycz − *Department of Physics, Center for Molecular Study of Condensed Soft Matter (μCoSM), Pritzker Institute of Biomedical Science and Engineering, Illinois Institute of Technology, Chicago, Illinois 60616, United States; X-ray Science Division, Argonne National Laboratory, Lemont, Illinois 60439, United States;* orcid.org/0000-0003-0055-230X

Ivan Kuzmenko − *X-ray Science Division, Argonne National Laboratory, Lemont, Illinois 60439, United States*

Wei Bu − *The Center for Advanced Radiation Sources (CARS), University of Chicago, Chicago, Illinois 60637, United States*

Stephen B. Hall − *Pulmonary & Critical Care Medicine, Oregon Health & Science University, Portland, Oregon 97239, United States;* orcid.org/0000-0001-8870-2143

Complete contact information is available at: https://pubs.acs.org/10.1021/acs.langmuir.0c01813

Author Contributions

K.A. and M.W.M. contributed equally to this work.

Notes

The authors declare no competing financial interest.

■ ACKNOWLEDGMENTS

The authors thank Dr. Edmund Egan (ONY, Inc., Amherst, NY) for the gift of CLSE. This research was supported by funds from the National Institutes of Health (HL130130 and 136734). This study used resources of the Advanced Photon Source, a U.S. Department of Energy (DOE) Office of Science User Facility operated for the DOE Office of Science by Argonne National Laboratory under contract no. DE-AC02-06CH11357. NSF's ChemMatCARS Sector 15 (beamline ID-15-C) is supported by the Divisions of Chemistry (CHE) and Materials Research (DMR), National Science Foundation, under grant number NSF/CHE-1834750.

■ REFERENCES

(1) Goerke, J.; Clements, J. A. Alveolar surface tension and lung surfactant. In *Handbook of Physiology—The Respiratory System Vol III, Part 1*; Macklem, P. T., Mead, J., Ed.; American Physiological Society: Washington, D.C., 1985; Vol. *III*, pp 247−261.

(2) Bastacky, J.; Lee, C. Y.; Goerke, J.; Koushafar, H.; Yager, D.; Kenaga, L.; Speed, T. P.; Chen, Y.; Clements, J. A. Alveolar lining layer is thin and continuous: low-temperature scanning electron microscopy of rat lung. *J. Appl. Physiol.* **1995**, *79*, 1615−1628.

(3) Fisher, M. J.; Wilson, M. F.; Weber, K. C. Determination of alveolar surface area and tension from in situ pressure-volume data. *Respir. Physiol.* **1970**, *10*, 159−171.

(4) Horie, T.; Hildebrandt, J. Dynamic compliance, limit cycles, and static equilibria of excised cat lung. *J. Appl. Physiol.* **1971**, *31*, 423−430.

(5) Schürch, S.; Goerke, J.; Clements, J. A. Direct determination of surface tension in the lung. *Proc. Natl. Acad. Sci. U.S.A.* **1976**, *73*, 4698−4702.

(6) Valberg, P. A.; Brain, J. D. Lung surface tension and air space dimensions from multiple pressure-volume curves. *J. Appl. Physiol.* **1977**, *43*, 730−738.

(7) Wilson, T. A. Relations among recoil pressure, surface area, and surface tension in the lung. *J. Appl. Physiol.* **1981**, *50*, 921−930.

(8) Smith, J. C.; Stamenovic, D. Surface forces in lungs. I. Alveolar surface tension-lung volume relationships. *J. Appl. Physiol.* **1986**, *60*, 1341−1350.

(9) Robertson, B. Pathology and pathophysiology of neonatal surfactant deficiency ("respiratory distress syndrome," "hyaline membrane disease"). In *Pulmonary Surfactant*, 1 ed.; Robertson, B., Van Golde, L. M. G., Batenburg, J. J., Eds.; Elsevier Science Publishers: Amsterdam, 1984; pp 383−418.

(10) Lachmann, B.; Robertson, B.; Vogel, J. In vivo lung lavage as an experimental model of the respiratory distress syndrome. *Acta Anaesthesiol. Scand.* **1980**, *24*, 231−236.

(11) Murray, J. F. *The Normal Lung: The Basis for Diagnosis and Treatment of Pulmonary Disease*; Saunders, 1976.
(12) Patlak, C. S.; Gershfeld, N. L. A theoretical treatment for the kinetics of monolayer desorption from interfaces. *J. Colloid Interface Sci.* **1967**, *25*, 503−513.
(13) Lee, S.; Kim, D. H.; Needham, D. Equilibrium and Dynamic Interfacial Tension Measurements at Microscopic Interfaces Using a Micropipet Technique. 2. Dynamics of Phospholipid Monolayer Formation and Equilibrium Tensions at the Water−Air Interface. *Langmuir* **2001**, *17*, 5544−5550.
(14) Gaines, G. L., Jr. *Insoluble Monolayers at Liquid−Gas Interfaces*; Interscience Publishers: New York, 1966; pp 147.
(15) Smith, R. D.; Berg, J. C. The collapse of surfactant monolayers at the air-water interface. *J. Colloid Interface Sci.* **1980**, *74*, 273−286.
(16) Rapp, B.; Gruler, H. Phase transitions in thin smectic films at the air-water interface. *Phys. Rev. A: At., Mol., Opt. Phys.* **1990**, *42*, 2215−2218.
(17) Rugonyi, S.; Biswas, S. C.; Hall, S. B. The biophysical function of pulmonary surfactant. *Respir. Physiol. Neurobiol.* **2008**, *163*, 244−255.
(18) Schürch, S.; Green, F. H. Y.; Bachofen, H. Formation and structure of surface films: captive bubble surfactometry. *Biochim. Biophys. Acta* **1998**, *1408*, 180−202.
(19) Sen, A.; Hui, S.-W.; Mosgrober-Anthony, M.; Holm, B. A.; Egan, E. A. Localization of lipid exchange sites between bulk lung surfactants and surface monolayer: freeze fracture study. *J. Colloid Interface Sci.* **1988**, *126*, 355−360.
(20) Haller, T.; Dietl, P.; Stockner, H.; Frick, M.; Mair, N.; Tinhofer, I.; Ritsch, A.; Enhorning, G.; Putz, G. Tracing surfactant transformation from cellular release to insertion into an air-liquid interface. *Am. J. Physiol.: Lung Cell. Mol. Physiol.* **2004**, *286*, L1009−L1015.
(21) Bachofen, H.; Hildebrandt, J.; Bachofen, M. Pressure-volume curves of air- and liquid-filled excised lungs-surface tension in situ. *J. Appl. Physiol.* **1970**, *29*, 422−431.
(22) Horie, T.; Ardila, R.; Hildebrandt, J. Static and dynamic properties of excised cat lung in relation to temperature. *J. Appl. Physiol.* **1974**, *36*, 317−322.
(23) Schürch, S.; Qanbar, R.; Bachofen, H.; Possmayer, F. The surface-associated surfactant reservoir in the alveolar lining. *Biol. Neonate* **1995**, *67*, 61−76.
(24) Smith, E. C.; Crane, J. M.; Laderas, T. G.; Hall, S. B. Metastability of a supercompressed fluid monolayer. *Biophys. J.* **2003**, *85*, 3048−3057.
(25) Al-Saiedy, M.; Tarokh, A.; Nelson, S.; Hossini, K.; Green, F.; Ling, C.-C.; Prenner, E. J.; Amrein, M. The role of multilayers in preventing the premature buckling of the pulmonary surfactant. *Biochim. Biophys. Acta* **2017**, *1859*, 1372−1380.
(26) Sachan, A. K.; Zasadzinski, J. A. Interfacial curvature effects on the monolayer morphology and dynamics of a clinical lung surfactant. *Proc. Natl. Acad. Sci. U.S.A.* **2018**, *115*, No. E134.
(27) Putz, G.; Goerke, J.; Clements, J. A. Surface activity of rabbit pulmonary surfactant subfractions at different concentrations in a captive bubble. *J. Appl. Physiol.* **1994**, *77*, 597−605.
(28) Veldhuizen, E. J. A.; Batenburg, J. J.; van Golde, L. M. G.; Haagsman, H. P. The role of surfactant proteins in DPPC enrichment of surface films. *Biophys. J.* **2000**, *79*, 3164−3171.
(29) Schürch, D.; Ospina, O. L.; Cruz, A.; Pérez-Gil, J. Combined and independent action of proteins SP-B and SP-C in the surface behavior and mechanical stability of pulmonary surfactant films. *Biophys. J.* **2010**, *99*, 3290−3299.
(30) Dagan, M. P.; Hall, S. B. The equilibrium spreading tension of pulmonary surfactant. *Langmuir* **2015**, *31*, 13063−13067.
(31) Nag, K.; Perez-Gil, J.; Ruano, M. L. F.; Worthman, L. A. D.; Stewart, J.; Casals, C.; Keough, K. M. W. Phase transitions in films of lung surfactant at the air-water interface. *Biophys. J.* **1998**, *74*, 2983−2995.
(32) Clements, J. A. Surface tension of lung extracts. *Proc. Soc. Exp. Biol. Med.* **1957**, *95*, 170−172.
(33) Als-Nielsen, J.; Jacquemain, D.; Kjaer, K.; Leveiller, F.; Lahav, M.; Leiserowitz, L. Principles and applications of grazing incidence X-ray and neutron scattering from ordered molecular monolayers at the air-water interface. *Phys. Rep.* **1994**, *246*, 251−313.
(34) Discher, B. M.; Maloney, K. M.; Schief, W. R., Jr.; Grainger, D. W.; Vogel, V.; Hall, S. B. Lateral phase separation in interfacial films of pulmonary surfactant. *Biophys. J.* **1996**, *71*, 2583−2590.
(35) Crane, J. M.; Hall, S. B. Rapid compression transforms interfacial monolayers of pulmonary surfactant. *Biophys. J.* **2001**, *80*, 1863−1872.
(36) Watkins, J. C. The surface properties of pure phospholipids in relation to those of lung extracts. *Biochim. Biophys. Acta* **1968**, *152*, 293−306.
(37) Clements, JA Functions of the alveolar lining. *Am. Rev. Respir. Dis.* **1977**, *115*, 67−71.
(38) Bangham, A. D.; Morley, C. J.; Phillips, M. C. The physical properties of an effective lung surfactant. *Biochim. Biophys. Acta* **1979**, *573*, 552−556.
(39) Kaganer, V. M.; Möhwald, H.; Dutta, P. Structure and phase transitions in Langmuir monolayers. *Rev. Mod. Phys.* **1999**, *71*, 779−819.
(40) Postle, A. D.; Heeley, E. L.; Wilton, D. C. A comparison of the molecular species compositions of mammalian lung surfactant phospholipids. *Comp. Biochem. Physiol., Part A: Mol. Integr. Physiol.* **2001**, *129*, 65−73.
(41) Ivankin, A.; Kuzmenko, I.; Gidalevitz, D. Cholesterol-phospholipid interactions: New insights from surface x-ray scattering data. *Phys. Rev. Lett.* **2010**, *104*, 108101.
(42) Discher, B. M.; Maloney, K. M.; Grainger, D. W.; Sousa, C. A.; Hall, S. B. Neutral lipids induce critical behavior in interfacial monolayers of pulmonary surfactant. *Biochemistry* **1999**, *38*, 374−383.
(43) Discher, B. M.; Maloney, K. M.; Grainger, D. W.; Hall, S. B. Effect of neutral lipids on coexisting phases in monolayers of pulmonary surfactant. *Biophys. Chem.* **2002**, *101−102*, 333−345.
(44) Ueda, S.; Ishii, N.; Matsumoto, S.; Hayashi, K.; Okayasu, M. Ultrastructural studies on surface lining layer of the lungs. Part II. *J. Jpn. Med. Soc. Biol. Interface* **1983**, *14*, 24−46.
(45) Hills, B. A. *The Biology of Surfactant*; Cambridge University Press: Cambridge, New York, 1988; pp 222−235.
(46) Neville, F.; Cahuzac, M.; Konovalov, O.; Ishitsuka, Y.; Lee, K. Y. C.; Kuzmenko, I.; Kale, G. M.; Gidalevitz, D. Lipid headgroup discrimination by antimicrobial peptide LL-37: Insight into mechanism of action. *Biophys. J.* **2006**, *90*, 1275−1287.
(47) Andreev, K.; Martynowycz, M. W.; Huang, M. L.; Kuzmenko, I.; Bu, W.; Kirshenbaum, K.; Gidalevitz, D. Hydrophobic interactions modulate antimicrobial peptoid selectivity towards anionic lipid membranes. *Biochim. Biophys. Acta* **2018**, *1860*, 1414−1423.
(48) Gidalevitz, D.; Ishitsuka, Y.; Muresan, A. S.; Konovalov, O.; Waring, A. J.; Lehrer, R. I.; Lee, K. Y. C. Interaction of antimicrobial peptide protegrin with biomembranes. *Proc. Natl. Acad. Sci. U.S.A.* **2003**, *100*, 6302−6307.
(49) Wu, G.; Majewski, J.; Ege, C.; Kjaer, K.; Weygand, M. J.; Lee, K. Y. C. Interaction between lipid monolayers and poloxamer 188: An X-ray reflectivity and diffraction study. *Biophys. J.* **2005**, *89*, 3159−3173.
(50) Schief, W. R.; Antia, M.; Discher, B. M.; Hall, S. B.; Vogel, V. Liquid-crystalline collapse of pulmonary surfactant monolayers. *Biophys. J.* **2003**, *84*, 3792−3806.
(51) Malcharek, S.; Hinz, A.; Hilterhaus, L.; Galla, H.-J. Multilayer structures in lipid monolayer films containing surfactant protein C: effects of cholesterol and POPE. *Biophys. J.* **2005**, *88*, 2638−2649.
(52) McConnell, H. M.; Vrljic, M. Liquid-liquid immiscibility in membranes. *Annu. Rev. Biophys. Biomol. Struct.* **2003**, *32*, 469−492.
(53) Discher, B. M.; Schief, W. R.; Vogel, V.; Hall, S. B. Phase separation in monolayers of pulmonary surfactant phospholipids at the air-water interface: composition and structure. *Biophys. J.* **1999**, *77*, 2051−2061.
(54) Andersson, J. M.; Grey, C.; Larsson, M.; Ferreira, T. M.; Sparr, E. Effect of cholesterol on the molecular structure and transitions in a

https://dx.doi.org/10.1021/acs.langmuir.0c01813
Langmuir 2020, 36, 13439−13447

clinical-grade lung surfactant extract. *Proc. Natl. Acad. Sci. U.S.A.* **2017**, *114*, E3592−E3601.
(55) Larsson, M.; Larsson, K.; Nylander, T.; Wollmer, P. The bilayer melting transition in lung surfactant bilayers: The role of cholesterol. *Eur. Biophys. J.* **2003**, *31*, 633−636.
(56) Larsson, M.; Nylander, T.; Keough, K. M. W.; Nag, K. An X-ray diffraction study of alterations in bovine lung surfactant bilayer structures induced by albumin. *Chem. Phys. Lipids* **2006**, *144*, 137−145.
(57) Colacicco, G.; Basu, M. K. Effects of cholesterol and cholesteryl ester on dynamic surface tension of dipalmitoyl lecithin. *J. Colloid Interface Sci.* **1977**, *61*, 516−518.
(58) Hildebran, J. N.; Goerke, J.; Clements, J. A. Pulmonary surface film stability and composition. *J. Appl. Physiol.* **1979**, *47*, 604−611.
(59) Notter, R. H.; Tabak, S. A.; Mavis, R. D. Surface properties of binary mixtures of some pulmonary surfactant components. *J. Lipid Res.* **1980**, *21*, 10−22.
(60) Gunasekara, L.; Schürch, S.; Schoel, W. M.; Nag, K.; Leonenko, Z.; Haufs, M.; Amrein, M. Pulmonary surfactant function is abolished by an elevated proportion of cholesterol. *Biochim. Biophys. Acta* **2005**, *1737*, 27−35.
(61) Veldhuizen, R.; Nag, K.; Orgeig, S.; Possmayer, F. The role of lipids in pulmonary surfactant. *Biochim. Biophys. Acta* **1998**, *1408*, 90−108.
(62) Lang, C. J.; Postle, A. D.; Orgeig, S.; Possmayer, F.; Bernhard, W.; Panda, A. K.; Jürgens, K. D.; Milsom, W. K.; Nag, K.; Daniels, C. B. Dipalmitoylphosphatidylcholine is not the major surfactant phospholipid species in all mammals. *Am. J. Physiol.: Regul., Integr. Comp. Physiol.* **2005**, *289*, R1426−R1439.
(63) Wilson, T. A. Surface tension-surface area curves calculated from pressure-volume loops. *J. Appl. Physiol.* **1982**, *53*, 1512−1520.
(64) Bachofen, H.; Schürch, S.; Urbinelli, M.; Weibel, E. R. Relations among alveolar surface tension, surface area, volume, and recoil pressure. *J. Appl. Physiol.* **1987**, *62*, 1878−1887.
(65) Schram, V.; Hall, S. B. Thermodynamic effects of the hydrophobic surfactant proteins on the early adsorption of pulmonary surfactant. *Biophys. J.* **2001**, *81*, 1536−1546.
(66) Loney, R. W.; Anyan, W. R.; Biswas, S. C.; Rananavare, S. B.; Hall, S. B. The accelerated late adsorption of pulmonary surfactant. *Langmuir* **2011**, *27*, 4857−4866.
(67) Mansour, H. M.; Zografi, G. Relationships between Equilibrium Spreading Pressure and Phase Equilibria of Phospholipid Bilayers and Monolayers at the Air−Water Interface. *Langmuir* **2007**, *23*, 3809−3819.
(68) Notter, R. H.; Finkelstein, J. N.; Taubold, R. D. Comparative adsorption of natural lung surfactant, extracted phospholipids, and artificial phospholipid mixtures to the air-water interface. *Chem. Phys. Lipids* **1983**, *33*, 67−80.
(69) Bligh, E. G.; Dyer, W. J. A rapid method of total lipid extraction and purification. *Can. J. Biochem. Physiol.* **1959**, *37*, 911−917.
(70) Hall, S. B.; Wang, Z.; Notter, R. H. Separation of subfractions of the hydrophobic components of calf lung surfactant. *J. Lipid Res.* **1994**, *35*, 1386−1394.
(71) Kahn, M. C.; Anderson, G. J.; Anyan, W. R.; Hall, S. B. Phosphatidylcholine molecular species of calf lung surfactant. *Am. J. Physiol.* **1995**, *269*, L567−L573.
(72) Kumar, K.; Chavarha, M.; Loney, R. W.; Weiss, T. M.; Rananavare, S. B.; Hall, S. B. The Lγ Phase of Pulmonary Surfactant. *Langmuir* **2018**, *34*, 6601−6611.
(73) Markin, C. J.; Dick, D. L.; Hall, S. B. Complete compositional analysis of phospholipids in calf pulmonary surfactant. *Am. J. Respir. Crit. Care Med.* **1999**, *161*, A896.
(74) Borie, B. X-ray diffraction in crystals, imperfect crystals, and amorphous bodies. *J. Am. Chem. Soc.* **1965**, *87*, 140−141.
(75) McGovern, I. T.; Norman, D.; Williams, R. H. Surface science with synchrotron radiation. In *Handbook on Synchrotron Radiation*; Marr, G. V., Ed.; Elsevier: Amsterdam, 1987; Vol. 2, pp 467−539.
(76) Jensen, T. R.; Kjaer, K. Structural properties and interactions of thin films at the air-liquid interface explored with syndhrotron X-ray scattering. In *Novel Methods to Study Interfacial Layers*, 1st ed.; Möbius, D., Miller, R., Eds.; Elsevier: Amsterdam; New York, 2001; pp 205−254.
(77) Tanaka, M.; Schneider, M. F.; Brezesinski, G. In-Plane Structures of Synthetic Oligolactose Lipid Monolayers-Impact of Saccharide Chain Length. *ChemPhysChem* **2003**, *4*, 1316−1322.
(78) Danauskas, S. M.; Li, D.; Meron, M.; Lin, B.; Lee, K. Y. C. Stochastic fitting of specular X-ray reflectivity data usingStochFit. *J. Appl. Crystallogr.* **2008**, *41*, 1187−1193.
(79) Braslau, A.; Pershan, P. S.; Swislow, G.; Ocko, B. M.; Als-Nielsen, J. Capillary waves on the surface of simple liquids measured by x-ray reflectivity. *Phys. Rev. A: At., Mol., Opt. Phys.* **1988**, *38*, 2457−2470.
(80) Andreev, K.; Bianchi, C.; Laursen, J. S.; Citterio, L.; Hein-Kristensen, L.; Gram, L.; Kuzmenko, I.; Olsen, C. A.; Gidalevitz, D. Guanidino groups greatly enhance the action of antimicrobial peptidomimetics against bacterial cytoplasmic membranes. *Biochim. Biophys. Acta* **2014**, *1838*, 2492−2502.
(81) Andreev, K.; Martynowycz, M. W.; Ivankin, A.; Huang, M. L.; Kuzmenko, I.; Meron, M.; Lin, B.; Kirshenbaum, K.; Gidalevitz, D. Cyclization improves membrane permeation by antimicrobial peptoids. *Langmuir* **2016**, *32*, 12905−12913.
(82) Andreev, K.; Martynowycz, M. W.; Gidalevitz, D. Peptoid drug discovery and optimization via surface X-ray scattering. *Biopolymers* **2019**, *110*, No. e23274.
(83) Nobre, T. M.; Martynowycz, M. W.; Andreev, K.; Kuzmenko, I.; Nikaido, H.; Gidalevitz, D. Modification of salmonella lipopolysaccharides prevents the outer membrane penetration of novobiocin. *Biophys. J.* **2015**, *109*, 2537−2545.
(84) Martynowycz, M. W.; Rice, A.; Andreev, K.; Nobre, T. M.; Kuzmenko, I.; Wereszczynski, J.; Gidalevitz, D. Salmonella membrane structural remodeling increases resistance to antimicrobial peptide LL-37. *ACS Infect. Dis.* **2019**, *5*, 1214−1222.
(85) Martynowycz, M. W.; Hu, B.; Kuzmenko, I.; Bu, W.; Hock, A.; Gidalevitz, D. Monomolecular siloxane film as a model of single site catalysts. *J. Am. Chem. Soc.* **2016**, *138*, 12432−12439.

https://dx.doi.org/10.1021/acs.langmuir.0c01813
Langmuir 2020, 36, 13439−13447